Spontaneous and electric field–controlled front–rear polarization of human keratinocytes

Deniz Saltukoglu[a,b,c,d], Julian Grünewald[a,b], Nico Strohmeyer[a,b,*], Robert Bensch[d,e], Maximilian H. Ulbrich[d,f], Olaf Ronneberger[d,e], and Matias Simons[a,b,d,g]

[a]Center for Systems Biology, [c]Spemann Graduate School of Biology and Medicine, and [d]BIOSS Centre for Biological Signalling Studies, University of Freiburg, 79104 Freiburg, Germany; [b]Renal Division, University Hospital Freiburg, and [f]Institute of Physiology II, University of Freiburg, 79106 Freiburg, Germany; [e]Institute for Computer Science, Faculty of Engineering, University of Freiburg, 79110 Freiburg, Germany; [g]Imagine Institute, Paris Descartes University–Sorbonne Paris Cité, 75015 Paris, France

ABSTRACT **It has long been known that electrical fields (EFs) are able to influence the direction of migrating cells, a process commonly referred to as electrotaxis or galvanotaxis. Most studies have focused on migrating cells equipped with an existing polarity before EF application, making it difficult to delineate EF-specific pathways. Here we study the initial events in front–rear organization of spreading keratinocytes to dissect the molecular requirements for random and EF-controlled polarization. We find that Arp2/3-dependent protrusive forces and Rac1/Cdc42 activity were generally required for both forms of polarization but were dispensable for controlling the direction of EF-controlled polarization. By contrast, we found a crucial role for extracellular pH as well as G protein coupled–receptor (GPCR) or purinergic signaling in the control of directionality. The normal direction of polarization toward the cathode was reverted by lowering extracellular pH. Polarization toward the anode was also seen at neutral pH when GPCR or purinergic signaling was inhibited. However, the stepwise increase of extracellular pH in this scenario led to restoration of cathodal polarization. Overall our work puts forward a model in which the EF uses distinct polarization pathways. The cathodal pathway involves GPCR/purinergic signaling and is dominant over the anodal pathway at neutral pH.**

Monitoring Editor
Fred Chang
Columbia University

Received: Dec 4, 2014
Revised: Aug 21, 2015
Accepted: Sep 21, 2015

INTRODUCTION

Externally applied DC EFs function as spatial cues to motile single cells or a monolayer of cells (Zhao *et al.*, 2006; Zhao, 2009; Chang and Minc, 2014; Cohen *et al.*, 2014). EFs have also been shown to induce directional growth in the fission yeast *Schizosaccharomyces pombe* (Minc and Chang, 2010) and to orient neurite growth of *Xenopus* neurons (Patel and Poo, 1982) and control the beating direction of cilia in *Paramecium* (Jahn, 1961). Moreover, vibrating-probe measurements have detected endogenous ionic currents at epithelial wound sites (Chiang *et al.*, 1992; Reid *et al.*, 2007), amputated limbs (Borgens *et al.*, 1977), and developing embryos (Jaffe and Stern, 1979; Hotary and Robinson, 1994). The measured currents seem to be in the same order of magnitude as the currents produced by electric field strengths required to induce directional cell behaviors in vitro (<100 mV/mm). Thus it is believed that they are capable of influencing morphogenesis and regeneration by steering cell migration (Levin, 2009; Zhao, 2009). In skin wounds, EFs are believed to arise due to the short-circuiting of the transepithelial potential under which keratinocytes move toward the wound center to reepithelialize it. Recent findings suggest that electrophoresis of membrane components represents the mechanistic basis of electrotaxis directionality (Allen *et al.*, 2013).

A key prerequisite for cell migration is the establishment of a front–rear polarization (Bourne and Weiner, 2002). Unpolarized cells need to break symmetry and form a lamellipodium at the front and a lagging edge at the back to initiate locomotion. While the lamellipodium provides the protrusive force, the lagging edge

This article was published online ahead of print in MBoC in Press (http://www.molbiolcell.org/cgi/doi/10.1091/mbc.E14-12-1580) on September 30, 2015.

*Present address: Department of Biosystems Science and Engineering, ETH Zürich, 4058 Basel, Switzerland.

Address correspondence to: Matias Simons (matias.simons@institutimagine.org).

Abbreviation used: EF, electrical field.

contracts to detach the cell from the substratum and drive forward translocation of the cell body (Lauffenburger and Horwitz, 1996). This kind of polarization can occur spontaneously or in response to external cues. With an electrical cue, it is unclear whether the directionality signal is generated at the anodal or the cathodal side or whether there is a fixed position. The preferred direction of cellular motility in vitro varies according to the cell type and also within one cell type, depending on the experimental conditions and the genetic background. Although most of the tested cell types migrate toward the cathode, some cell types have been reported to move toward the anode (Ferrier *et al.*, 1986; Rapp *et al.*, 1988; Soong *et al.*, 1990). Lens epithelial cells can move anodally or cathodally, depending on the electric field strength (Wang *et al.*, 2003). Fish keratocytes move to the cathode, whereas spontaneously detaching cell fragments move to the anode (Sun *et al.*, 2013). Further, the genetic manipulation of the cGMP and phosphatidylinositide 3-kinase (PI3K) pathways, as well as the plasma membrane proton pump pma1, can reverse the direction of EF responses in *Dictyostelium discoideum* (Sato *et al.*, 2009) and *S. pombe* (Minc and Chang, 2010), respectively. Taken together, the reversal phenotypes are an indication that more than one and perhaps competing signaling pathways are involved in directionality determination (Sato *et al.*, 2009; Sun *et al.*, 2013).

Due to the high resistance of the plasma membrane, it is believed that the most upstream sensing mechanism(s) should be situated at the outer surface of the cell. Accordingly, several cell surface receptors (e.g., epidermal growth factor [EGF] receptor, vascular endothelial growth factor receptor, β2-adrenergic and purinergic receptors; Fang *et al.*, 1999; Zhao *et al.*, 2004, 2006; Pullar and Isseroff, 2005; Pu *et al.*, 2007; Riding and Pullar, 2015) and ion channels and exchangers (e.g., epithelial sodium channel, sodium-proton exchanger 1; Zhao *et al.*, 2006; Yang *et al.*, 2013) have been shown to be involved in response to external EFs. So far, however, it has been possible neither to denominate the molecular requirements across different cell types nor to dissect whether there are one or many dedicated EF sensors. At the level of intracellular signaling, EF shares features with the pathways governing chemotaxis or any other cell migration type (Zhao *et al.*, 2006; Allen *et al.*, 2013). It is important to point out that a common procedure is to apply the EF to migrating cells, leading to reorientation of the migration direction. Although this allows the study of turning behavior, insights into EF sensing and polarization mechanisms may be impaired by potential amplification mechanisms and feedback loops established in migrating cells before EF application.

In this study, we developed an assay to follow symmetry breaking of human keratinocytes into a front–rear polarity. The direction of polarization is random without the EF and directional with the EF. Using this reductionist assay, we tested the role of a panel of molecules involved in polarization, ranging from intracellular cytoskeletal regulators to cell surface receptors. Our findings suggest that spontaneous symmetry breaking depends on cytoskeletal elements, which can be used by polarization pathways sensing the EF. We also demonstrate that polarization is normally toward the cathode in keratinocytes, but the direction can be randomized or reversed by lowering extracellular pH and inhibiting G protein coupled–receptor (GPCR) and purinergic signaling. Our findings provide novel insights into the initial steps of front–rear polarization and pH-dependent directional responses.

RESULTS

Keratinocyte polarization assay to study symmetry breaking

Keratinocytes plated on a collagen type I surface acquire a distinct front–rear polarity with clearly defined leading and lagging edges. This kind of polarization is achieved via spontaneous symmetry breaking after attachment and spreading. To synchronize symmetry breaking in a group of single cells, we performed an assay that we named the "polarization assay" (Figure 1A). We rounded cells by incubating them in experiment medium containing 8% dimethyl sulfoxide (DMSO) for 30 min, followed by a medium wash. DMSO treatment leads to temporary lamellipodial loss and cell rounding, from which cells recover quickly after washout (Keren *et al.*, 2008; Sanger *et al.*, 1980). As cells regain volume, they spread uniformly on the substrate, producing a lamellipodium-like membrane structure encircling the cell body. Ninety-six percent of keratinocytes broke symmetry after spreading, and this was followed by migratory activity (Figure 1B and Supplemental Movie S1). Cells required an average of 48 min to break symmetry after the DMSO washout (Figure 1C). To test the external requirements for polarization, we removed the supplements recombinant EGF and bovine pituitary extract from the medium at the time of DMSO washout or 5 h before the experiment. No statistically significant difference in obtaining a stable polarity axis was observed, and the time needed to achieve symmetry breaking remained similar (Figure 1C).

To study the extent of migration after the initial polarization induced with the assay, we followed migration trajectories for 1.5 h and quantified track length, displacement, and straightness index (Supplemental Figure S1). Cells in supplemented medium migrated on average four cell lengths in the 1.5-h time frame. The track length and displacement significantly decreased for cells that were starved for 5 h before the experiment. In all conditions, cells followed straight paths during the time of recording.

Thus the polarization assay allows the quantification of spontaneous polarization and subsequent migration.

Control of polarization direction by the electric field

To test whether the direction of symmetry breaking can be controlled by external cues, we next applied an exogenous EF of 100 mV/mm during spreading and polarization phases. The direction of polarization was quantified within the 1.5 h of EF application after the washout of DMSO. In 70% of cases, the EF-directed polarization toward the quarter facing the cathode compared with the random polarity axis determination in control cells (Figure 1D and Supplemental Movie S2). There was no significant difference in the time it took for cells to polarize between the two conditions, implying that the internal polarization mechanism is the time-limiting factor in the dynamics of symmetry breaking (Figure 1C). The EF did not seem to change cell morphologies during polarization but slightly enhanced the stability of the polarity axis (Figure 1B).

To test the degree of electrotaxis after cell polarization, we further followed migration trajectories after symmetry breaking (Supplemental Figure S2). Whereas control cells had a directionality index, $\cos\theta$, close to 0, the value rose to 0.66 by applying the EF. The increase in the straightness index further shows that the electric field suppresses the angular deviations in the migration trajectories.

In sum, EF application can potently control the direction of both polarization and migration in keratinocytes.

The role of force generator molecules and small GTPases in spontaneous and directional polarization

Because the organization of the actin cytoskeleton is central to the formation of a front–rear asymmetry (Li and Gundersen, 2008), we imaged the actin cytoskeleton of cells with LifeAct-mCherry as they broke symmetry (Supplemental Movie S3). Live imaging revealed a dynamic reorganization of the actin cytoskeleton during polarization. During spreading, the actin cytoskeletal network was

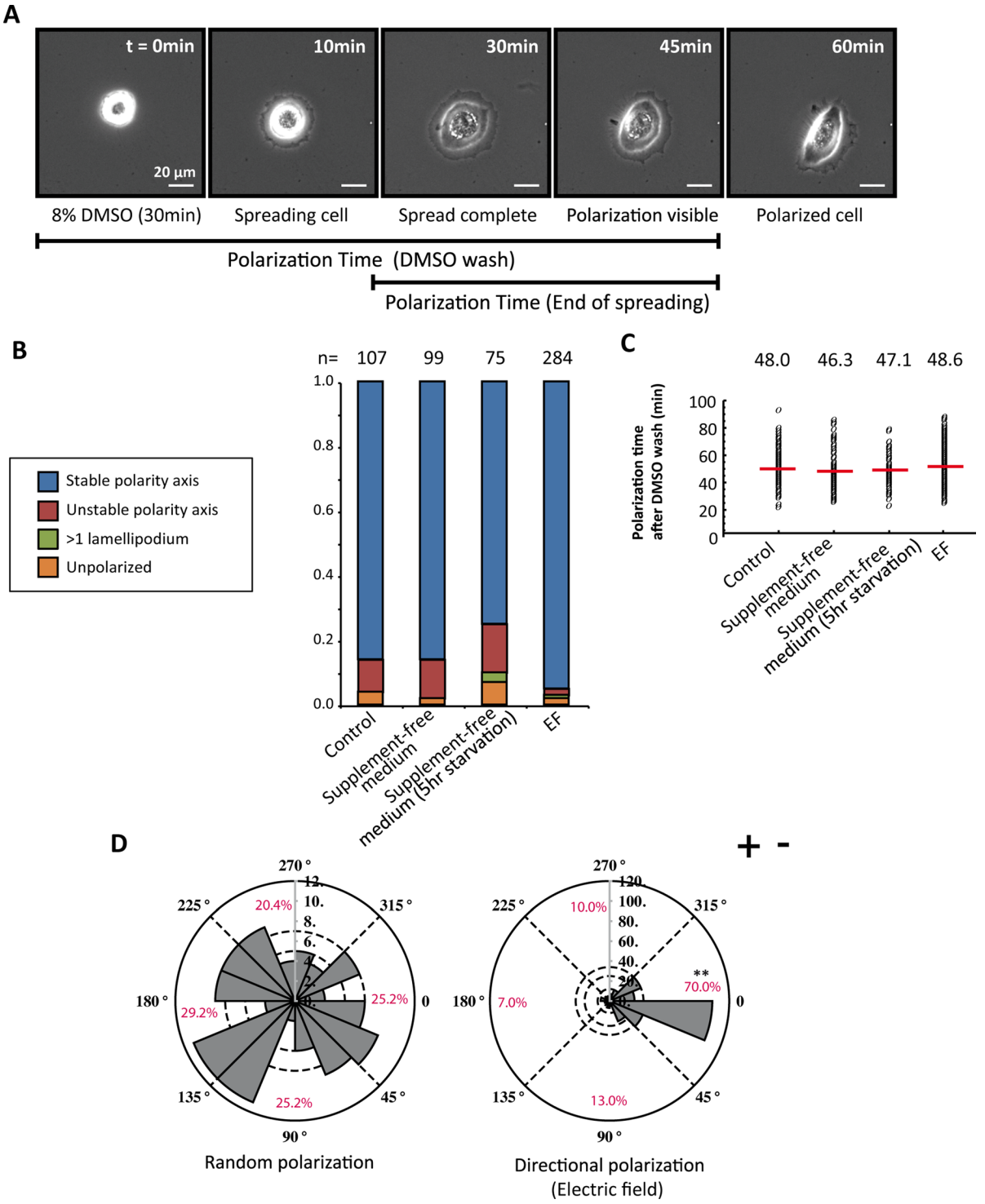

FIGURE 1: Keratinocytes efficiently break symmetry in the polarization assay. (A) Representative cell undergoing polarization assay. The first image in the time series shows the rounded morphology of the cell after being subjected to 8% DMSO–containing experiment medium for 30 min and marks the starting point (0 min) for the time quantification. At image 3, the cell has completely spread, with a lamellipodium-like membrane structure around the cell body. Symmetry breaking is visible at 45 min and completed by 60 min. (B) Classification of cell morphologies after cells broke symmetry and bar chart of morphologies for supplemented and unsupplemented medium. The number of cells quantified is indicated above each column. (C) Quantification of the time it takes for symmetry breaking after the DMSO is removed. Single dots represent single cells. The red line is the average value for each condition. (D) Rose plots representing the direction of symmetry breaking for random (left) and EF-controlled (right) polarization. The length of the gray pie slices corresponds to the number of cells belonging to the particular angular slice. The percentages are given for four different quarters, represented by dashed lines. Without the extracellular cue, cells are randomly polarizing. When cells are subjected to EF, 70% define their polarity axes with their lamellipodia facing the cathode (–). The *p* value is calculated with Student's t-test. $^{**}p < 0.01$.

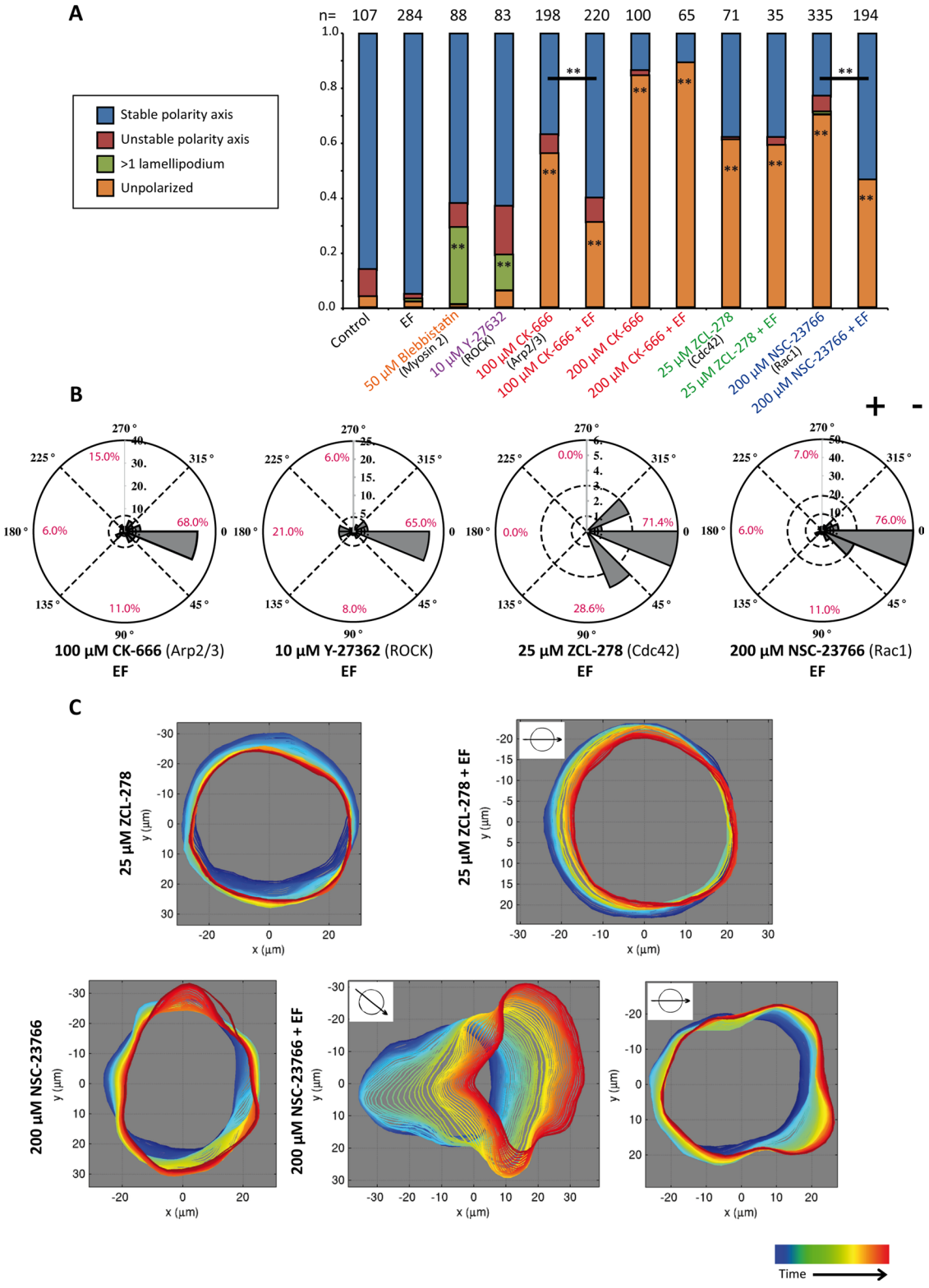

FIGURE 2: The role of cytoskeletal regulators in spontaneous and directional polarization. (A) Quantification of polarization phenotypes for inhibition of cytoskeletal force generators (myosin II [blebbistatin] and ROCK [Y-27362] for contractile rear and Arp2/3 complex [CK-666] for protrusive front) and inhibition of small GTPases Cdc42 (ZCL-278) and Rac1 (NSC-23766). Inhibiting the Arp2/3 complex, Cdc42, and Rac1 leads to the loss of symmetry breaking, whereas ROCK and myosin II inhibition generates cells with more than one lamellipodium. The EF significantly increases the percentage of cells breaking symmetry in the Arp2/3 and Rac1 inhibition conditions. The number of cells quantified is indicated above each column. The *p* value is calculated with Student's t test. $^{**}p < 0.01$. (B) Rose plots representing the direction of symmetry breaking of polarizing cells with the indicated inhibitors. (C) Automated boundary detection from phase contrast videos for the representative cells with the indicated treatments. Time progression is represented from

organized as a ring of parallel actin bundles surrounding the cell body. Subsequently cells spontaneously broke the symmetry of the actin ring by tightly pulling together the bundles within one-half of the cell, leading to the formation of the lagging edge. In the other half of the cell, the bundles expanded, leading to the formation of transverse actin arcs and the lamellipodium.

As a next step, we inhibited force generators of the actin network. The rear contractile system was inhibited with blebbistatin (nonmuscle myosin II inhibitor) or Y-27632 (Rho kinase [ROCK] inhibitor), and the protrusive front system was inhibited with CK-666 (Arp2/3 complex inhibitor). Both blebbistatin and Y-27632 significantly increased the percentage of cells with more than one lamellipodial structure but did not interfere with their symmetry-breaking ability (Figure 2A and Supplemental Figure S4B). The efficiency of Y-27632 treatment was confirmed by testing the reduction of doubly phosphorylated myosin regulatory light chain (ppMRCLC2) compared with untreated cells via immunoblotting (Supplemental Figure S4A). By contrast, Arp2/3 complex inhibition led to only 44 and 16% (using 100 or 200 μM CK-666, respectively) of cells being able to break symmetry, compared with 96% of cells in the control case (Figure 2A). Moreover, migration tracks were decreased in length by CK-666 treatment (Supplemental Figure S3B). Morphologically, inhibition of the Arp2/3 complex resulted in unpolarized cells with filopodia-like boundaries (Supplemental Figure S3B). Phalloidin staining revealed that the actin cytoskeleton was disorganized upon CK-666 treatment (Supplemental Figure S3C). In particular, the transverse arcs were reduced, and the direction of actin bundles was perpendicular to the cell periphery rather than parallel. Neither the reduction in polarization nor the loss of transverse arcs was seen with the inactive CK-666 analogue CK-689 (Supplemental Figure S3, A and C). Together these results demonstrate that Arp2/3 complex–dependent cytoskeleton rearrangements and protrusive forces at the cell periphery are key for breaking symmetry in keratinocytes, whereas myosin II– and ROCK-based contractility is not required.

Cdc42 and Rac1 are molecular switches that orchestrate the organization of the actomyosin cytoskeleton and regulate the activities of cytoskeletal force generators (Jaffe and Hall, 2005). Whereas Cdc42 is a key molecule in polarity establishment, Rac1 controls the formation of the lamellipodium (Heasman and Ridley, 2008). Cdc42 and Rac1 inhibition was performed with the drugs ZCL-278 and NSC-23766, respectively (Gao *et al.*, 2004; Friesland *et al.*, 2013). Both of these drugs reduced symmetry breaking in keratinocytes but produced different morphologies (Figure 2A and Supplemental Figure S3B). Cdc42 inhibition led to the apparent loss of protrusive activity, which was confirmed by automated outlining of the cellular boundary over time during the polarization assay (Figure 2C and Supplemental Movie S4). By contrast, Rac1 inhibition led to small but detectable protrusions occurring randomly at the cell periphery (Figure 2C, Supplemental Figure S4B, and Supplemental Movie S5).

Taken together, these data indicate that symmetry breaking in keratinocytes requires a protrusive Arp2/3-dependent actin network growth rather than a contractile rear. Whereas Cdc42 decreased the overall ability of cells to make protrusions, Rac1 was required to organize the stability and the size of protrusions to form a stable leading edge.

The electric field increases polarization in cells with compromised cytoskeletal signaling

We next tested the requirements for cytoskeletal force generators and small GTPases Cdc42 and Rac1 in EF-controlled polarization. For this, we quantified the direction of polarization in the cells that showed polarization under the treatment. The polarizing cells were also affected by the treatment, as they showed prolonged polarization times compared with control cells (unpublished data). Of interest, neither the inhibition of the cytoskeleton force generation with Y-27632 (contractile) nor with CK-666 (protrusive) affected the cathodal directionality of cells (Figure 2B). We further found that at a low concentration of CK-666 (100 μM), EF application increased the percentage of cells that were able to break symmetry (from 44 to 69%; Figure 2A). However, at a higher concentration (200 μM), this enhancement did not occur, as this treatment already inhibited the ability of cells to break symmetry, with 84% of cells staying unpolarized in the non-EF condition.

Similarly, the inhibition of the small GTPases Cdc42 and Rac1 did not affect directionality determination (Figure 2B). However, as for the Arp2/3 complex, EF stimulation raised the percentage of symmetry breaking in Rac1-inhibited cells from 30% (without EF) to 54% (with EF; Figure 2A). By extracting the cellular outlines over time, we could further demonstrate how EF could increase symmetry breaking in Rac1-inhibited cells. This may occur via the clustering of the uncoordinated protrusive activity, and therefore also of the protrusive force essential for symmetry breaking, toward the cathodal side (Figure 2C and Supplemental Movies S6 and S7). By contrast, the EF was unable to enhance symmetry breaking in Cdc42-inhibited cells, where all peripheral protrusions were suppressed (Figure 2C and Supplemental Movie S8).

Taken together, these findings show that the cytoskeleton force generators and cytoskeleton regulators are not responsible in directionality determination and that in some conditions, EF application can partially restore the capacity to polarize.

Plasma membrane signaling in spontaneous and directional polarization

As a next step, we inhibited more-upstream mediators of cell migration during both spontaneous and directional polarization. We selected a number of treatments that have been shown to affect directionality in electrotaxis. We first tested the PI3K system, which controls the formation of opposing gradients of the polarity lipids phosphatidylinositol (3,4,5)-trisphosphate (PIP3) and phosphatidylinositol (4,5)-bisphosphate (PIP2) in response to external cues (Bourne and Weiner, 2002). In addition, PIP3 is known to form positive feedback loops with Rac1 to induce lamellipodium formation (Srinivasan *et al.*, 2003). PI3K was inhibited with PIK-90, which targets three of four class I PI3K isoforms with equal selectivity (Knight *et al.*, 2006). Without the EF, PIK-90–treated cells broke symmetry but only to retract the newly created lamellipodia and form them at another location (Figure 3A and Supplemental Figure S3C). Treatment efficacy was tested by Western blot, which showed reduction of pAKT in cells treated with 5 μM PIK-90 (Supplemental Figure S4A). Inhibition of PI3K did not lead to the absence of lamellipodium formation, but its activity exerted a stabilizing effect on the position of

blue to red. In Cdc42-inhibited cells, EF does not induce any protrusions toward the cathode, and the percentage of cells breaking symmetry does not increase with EF. Rac1-inhibited cells show small, unsustained, and random boundary protrusions without EF. Two examples are shown for Rac1-inhibited cells with EF. In the left example, the cell clearly polarizes to the cathode. In the right example, small protrusions are driven toward the cathode and suppressed at the anodal side.

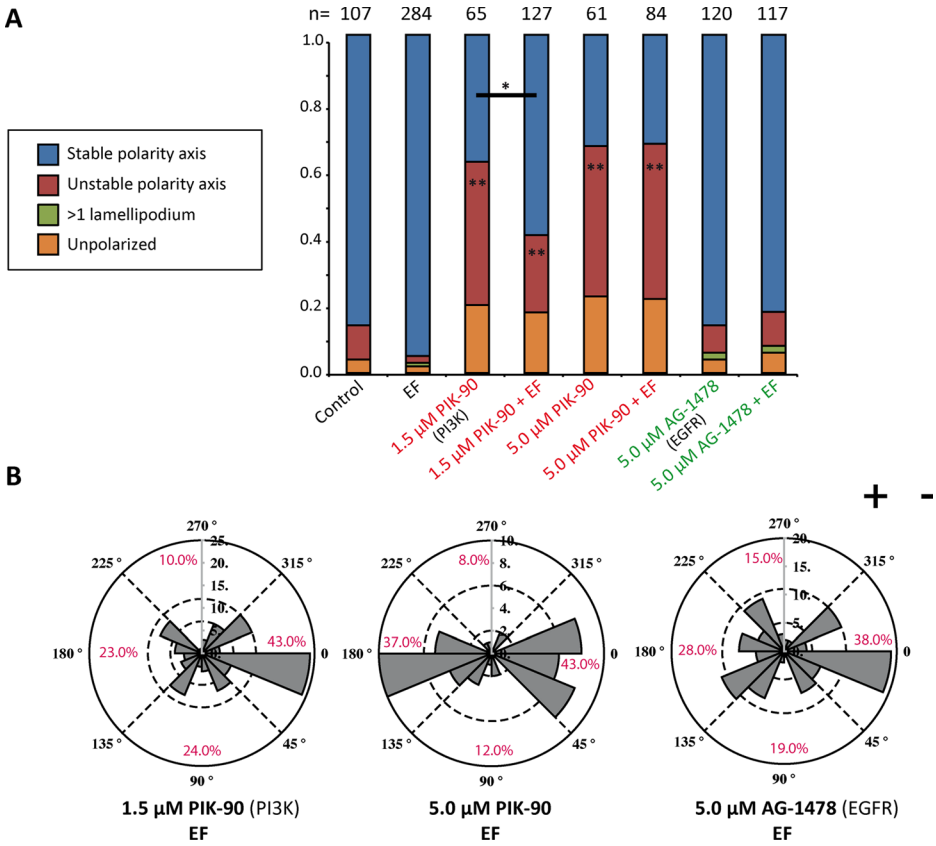

FIGURE 3: PI3K and EGFR inhibition in spontaneous and directional polarization. (A) Quantification of cell morphologies for PI3K (PIK-90) and EGFR (AG-1478) inhibition. PI3K inhibition leads to cellular morphology with an unstable polarity axis. At 1.5 µM PIK-90, the EF can partially rescue this phenotype. The number of cells quantified is indicated above each column. The *p value* is calculated with Student's *t* test. *$p < 0.05$, **$p < 0.01$. (B) Rose plots representing the direction of symmetry breaking with indicated inhibitors and doses. Whereas PI3K inhibition partially reverses the polarization direction, EGFR inhibition causes randomization.

the lamellipodium. EF application led to a partial rescue of the unstable polarity axis phenotype when using the lower PIK-90 concentration (1.5 µM). Moreover, PI3K inhibition partially reversed directionality. For the higher concentration of PIK-90 used (5 µM), cathodal directionality decreased from 70 to 43% and anodal directionality increased from 7 to 37% (Figure 3B). These results suggest that PI3K signaling is crucial for control of the polarization direction, consistent with its reported role in electrotaxis (Zhao *et al.*, 2006).

Next we turned to the EGF receptor tyrosine kinase (EGFR), which is a key molecule for directional motility in keratinocytes (Zhao *et al.*, 2002b; Ho and Dagnino, 2012). The EGFR inhibitor AG-1478 reduced the phosphorylation of EGFR but did not affect symmetry breaking (Figure 3A and Supplemental Figure S4, A and C). This is in accord with the normal polarization in medium without EGF supplementation (Figure 1B). In EF-controlled polarization, however, EGFR inhibition led to a significant randomization of directionality (Figure 3B), with cathodal polarization decreasing to 38%.

GPCRs comprise another class of receptors that have been associated with electrotaxis in various cell types (Zhao *et al.*, 2002a; Cao *et al.*, 2013). Among them is the purinergic P2Y receptor family, which has recently also been implicated in keratinocyte electrotaxis (Riding and Pullar, 2015). We used several compounds to inhibit both GPCR and P2 receptor signaling: pertussis toxin (PTX) for Gαi inhibition, gallein for Gβγ inhibition, telenzepine for the muscarinic M1 subclass of GPCRs, suramin and pyridoxal-phosphate-6-azophenyl-2′,4′-disulfonic acid (PPADS) for P2Y and P2X receptor inhibition. In addition to its antipurinergic effect, suramin also impairs general G protein coupling to GPCRs (Beindl *et al.*, 1996). None of these treatments impaired the ability for spontaneous polarization (Figure 4A). PTX led to a reduction of cathodal polarization, and a significant portion of cells showing a randomized response. Whereas telenzepine had no effect on directionality, PPADS led to a similar randomization of polarization as PTX. Strikingly, treatment with suramin and gallein completely reversed the direction of symmetry breaking from the cathode to the anode (Figure 4, B and C).

Taken together, these results show that PI3K, EGFR, GPCR, and purinergic signaling associated with the plasma membrane have important roles in directionality determination during keratinocyte polarization.

Low extracellular pH reverses the direction of polarization

Another way to influence directionality in electrotaxis is through change in extracellular pH. This effect has been proposed to be due to the change in charge on the surface of the plasma membrane (Allen *et al.*, 2013). Therefore we examined the effect of acidifying the extracellular pH (pH_e) to 6.6 in our system. Although this treatment slightly reduced the ability of the cells to polarize, it

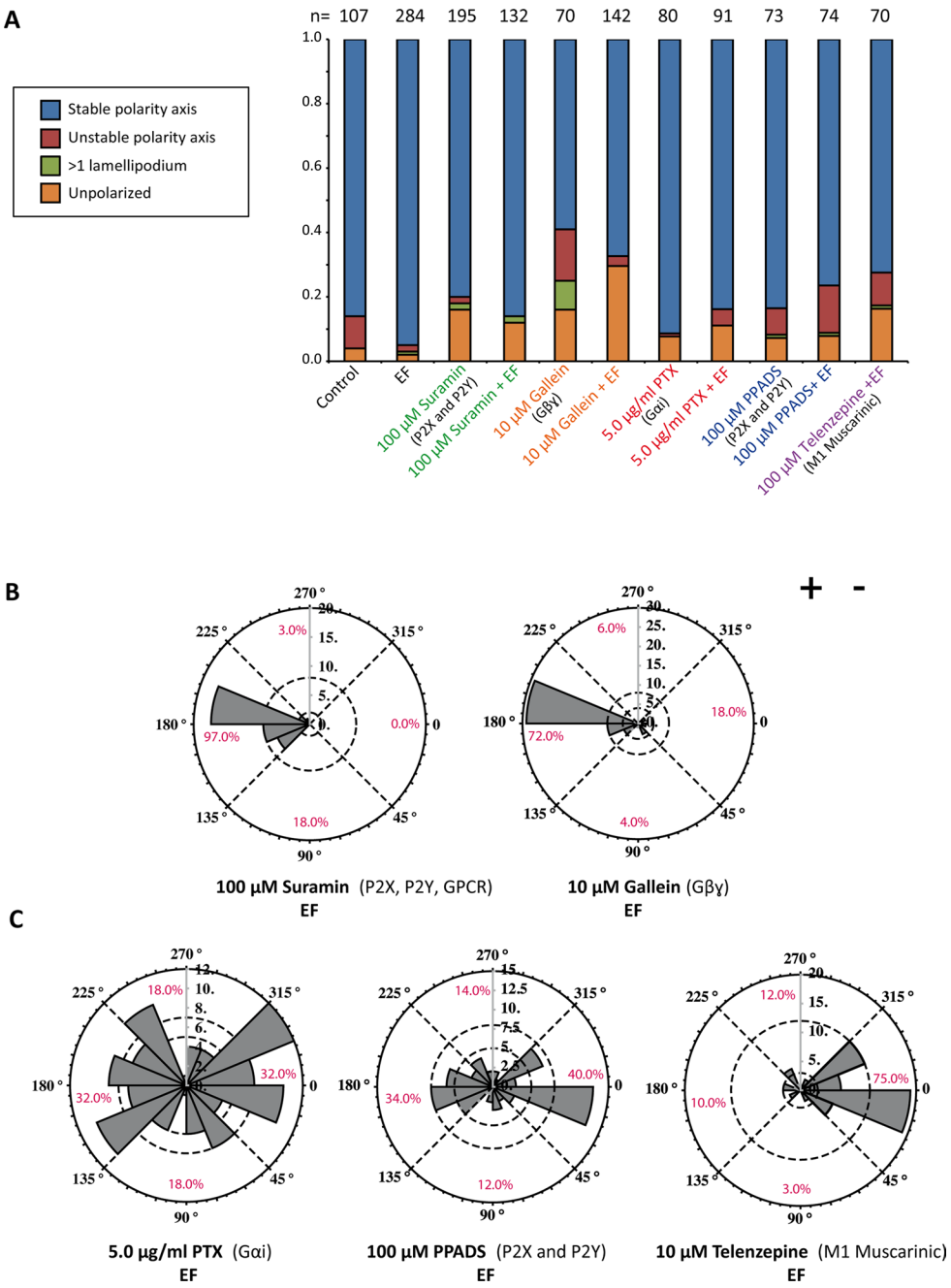

FIGURE 4: GPCR signaling in directional polarization. (A) Quantification of cell morphologies for inhibition of Gαi (PTX), Gβγ (gallein), purinergic signaling (suramin [also GPCR inhibition] and PPADS), and M1 muscarinic GPCR (telenzepine). None of the inhibitors, except for gallein to an extent, showed a significant effect on cell morphology. The number of cells quantified is indicated above each column. (B, C) Rose plots representing the direction of symmetry breaking with indicated inhibitors and doses. Whereas inhibiting Gαi with PTX treatment randomizes polarization, Gβγ inhibition reverses the direction of polarization toward the anode. At the receptor level, suramin reverses the direction of polarization, and PPADS leads to randomization of direction. Inhibiting the M1 muscarinic GPCR has no effect on the direction of polarization.

also led to reversal of the polarization direction, with 79% of all cells polarizing toward the anode (Figure 5, A and B, and Supplemental Movie S9). After migration, trajectories revealed that the cells that polarized toward the anode were still able to electrotax toward the anode (Supplemental Figure S5, A and B). In low pH_e, cells had a directionality index of –0.54, compared with 0.66 for cells in normal-pH medium. Nonetheless, anodal migration was less efficient than cathodal migration, with significantly lower average track length, straightness, and displacement value (Supplemental Figure S5, C–E).

Because the intracellular pH (pH_i) can also change when pH_e is lowered, we transiently transfected the cells with superecliptic pHluorin-mCherry, a genetically encoded, ratiometric pH sensor, to measure pH_i (Supplemental Figure S6, A–C; Koivusalo *et al.*, 2010).

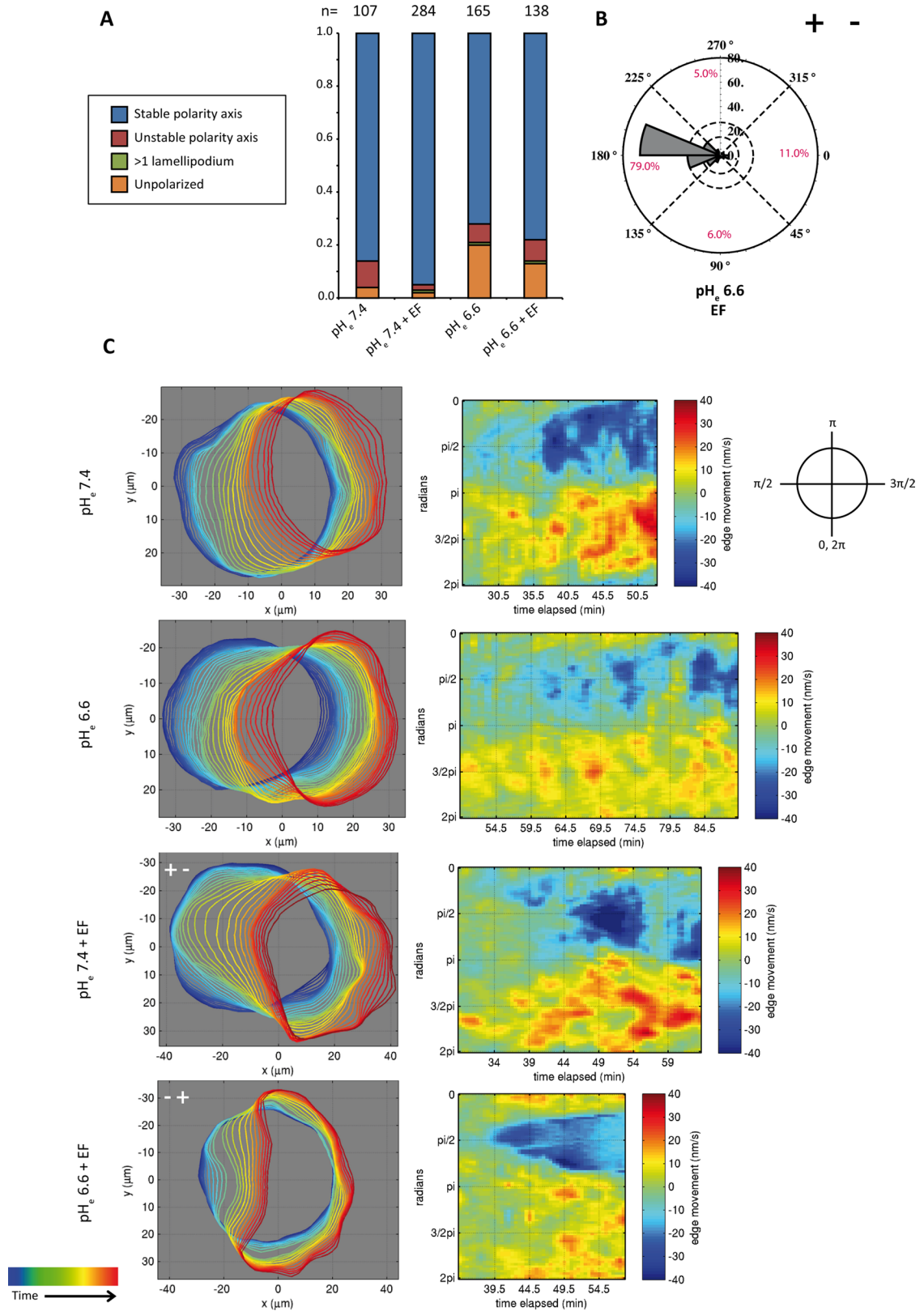

FIGURE 5: Lowering pH_e reverses the direction of symmetry breaking. (A) Quantification of morphologies of cells bathing in low pH_e with and without EF. The number of cells quantified is indicated above each column. (B) Rose plot representing the direction of symmetry breaking in low-pH medium. (C) Automated boundary detection from phase contrast videos and the associated protrusion/retraction maps constructed from boundary movements in time for the conditions of low- and normal-pH medium with and without EF. In the detected boundaries, time progression is represented from blue to red. In the protrusion/retraction maps, the *x*-axis represents the time, and the *y*-axis is the position of the cellular boundary from 0 to 2π. Representative cells have been turned at the indicated angles so that

Whereas the reduction of pH_e to 6.5 lowered pH_i by an average of 0.3 U, EF application did not cause any changes in pH_i in keratinocytes (Supplemental Figure S6, A and B). We also compared pH_i values at the anodal- and cathodal-facing cortical regions of cells. We did not detect any internal pH gradients that could be responsible for promoting polarization and directionality (Supplemental Figure S6, C and D; Martin *et al.*, 2011). By using the membrane-impermeable 2′,7′-bis(2-carboxyethyl)-5(6)-carboxyfluorescein (BCECF) acid, we further ruled out that the EF changes pH_e during the course of the experiment or induces a pH_e gradient in the chamber (Supplemental Figure S6, E and F). Together these results suggest that the extracellular pH is crucial for EF-mediated responses and that altered mobility of surface molecules could indeed be responsible for directionality. Although the acidification of pH_i may also contribute to the reversal of polarization, EF application changed neither pH_i nor pH_e.

Morphological differences in anodal and cathodal polarization

To understand the reversal of polarization with low pH_e further, we used protrusion/retraction maps to compare the morphology of symmetry-breaking cells in normal and low pH_e. In normal pH_e, before any movement in the position of the future lagging edge, cells protruded their plasma membrane toward the cathode (in the protrusion/retraction map, this can be seen as red spots before the event of actual symmetry breaking). This type of leading-edge protrusion was lacking in the low-pH medium condition. By contrast, an invagination of the back preceded the leading- edge protrusion. Initially, this invagination started in the midpoint of the future lagging edge and extended laterally with time, forming the characteristic conical shape of the blue areas representing retraction in the protrusion/retraction map (Figure 5C). Leading-edge protrusion and cell translocation during polarization were generally slower in this condition. Of importance, this type of symmetry breaking was not a general feature of cells in low-pH medium, as it was not observed in low pH_e without EF stimulation (Figure 5C and Supplemental Movie S10).

The morphological difference in the mode of symmetry breaking for cathodal and anodal polarization suggested that there may be a distinct set of cytoskeletal regulators responsible for either type of polarization. However, as with normal pH_e the inhibition of the Arp2/3 complex and ROCK at low pH_e did not lead to any changes to the direction of polarization (Supplemental Figure S7). These results further underscore that cytoskeleton elements are not determining the direction of polarization. Moreover, the observed changes in pH_i upon pH_e reduction do not seem to affect the cytoskeletal organization in polarizing cells.

Interplay of membrane signaling with pH_e in the EF response

Finally, we tested different pH conditions for the pharmacological treatments affecting directionality. We focused on the inhibitions of GPCR and purinergic signaling. For the treatments that cause reversal at normal pH_e (suramin and gallein), we observed anodal polarization at pH_e 6.6, 7.0, and 7.8, with restoration of cathodal polarization at pH_e 8.0 (Figure 6, A, B, and F). This suggests that the threshold for cathodal polarization can be pushed toward alkaline pH_e values when GPCR and purinergic signaling is inhibited. For the treatments that cause randomization at neutral pH_e (PTX and PPDS), we found anodal polarization at low pH_e and cathodal polarization at high pH_e (Figure 6, C, D, and F). Considering that randomization could be an intermediate step when switching from anodal to cathodal polarization, we predicted that a mildly acidic pH_e would cause randomization in untreated cells. This was indeed the case: randomization was found for untreated cells at pH_e 7.0. At pH_e 8.0, on the other hand, cathodal polarization was 10% more efficient than at normal pH_e (Figure 6, E and F).

Taken together, our results suggest a tug-of-war mechanism for directionality that is controlled by an interplay between surface signaling and pH_e. Whereas cathodal polarization dominates at neutral pH_e, randomization is a result of equally strong anodal and cathodal polarization pathways at slightly acidic pH_e.

DISCUSSION

Even though EF-generated directional responses have been studied for decades, little is known about the underlying mechanisms. The quest for a unifying view has been hampered by the fact that different cell lines seem to have different requirements for EF-induced directionality. Moreover, most electrotaxis studies have focused on how cells reorient, and there is—at least for mammalian cells—no direct assay to study how they establish their very first polarity when exposed to an EF. Using an assay for EF-guided cell polarization, we studied mechanisms of front–rear polarity generation and EF sensing in human keratinocytes. Compared to electrotaxis, this assay eliminated the complexity of revoking the previously established morphological and biochemical polarity of migratory cells because it generated a polarized cell from a uniform geometry. This not only led to a more robust directional response than in electrotaxis, but it also allowed us to study general polarization mechanisms in a hierarchical manner.

For cell polarization without EF, we found that PI3K signaling was key to a stable polarity axis but was not essential for asymmetry formation. This implies that these processes are regulated separately. Although Cdc42 and Rac1 GTPases were both indispensable for symmetry breaking, there were differences in their morphological phenotypes. Cdc42-inhibited cells did not show any protrusive activity at the cellular boundary after spreading. However, Rac1-inhibited cells protruded at the cellular boundary, which was marked with small and random protrusions, albeit not strong and coordinated enough to polarize the cells. Accordingly, the inhibition of the Arp2/3 complex, which regulates the branching of actin filaments at the leading edge, abolished any symmetry-breaking and protrusive activity. The inhibition of contractile forces mediated by myosin II, on the other hand, failed to block symmetry breaking. Cells could not keep a rigid and intact shape and had larger lamellipodia accompanied by frequent lamellipodium breaks. These results demonstrate that the protrusive force but not the contractile back is key to symmetry breaking in keratinocytes. This is in contrast to fish keratocytes, which were shown to require myosin-based rear

their leading edges always face the right side. Symmetry breaking in the normal-pH condition (with and without EF), as well as low-pH condition (without EF), is featured by front protrusions preceding the retraction of the back. By contrast, at low pH (with EF), there is an invagination of the cellular boundary at the lagging edge. The invagination event is represented by the unique conical shape of the blue retraction area of the corresponding protrusion/retraction map. Moreover, there is also a general reduction of leading-edge protrusion and cell translocation speed during polarization in this condition.

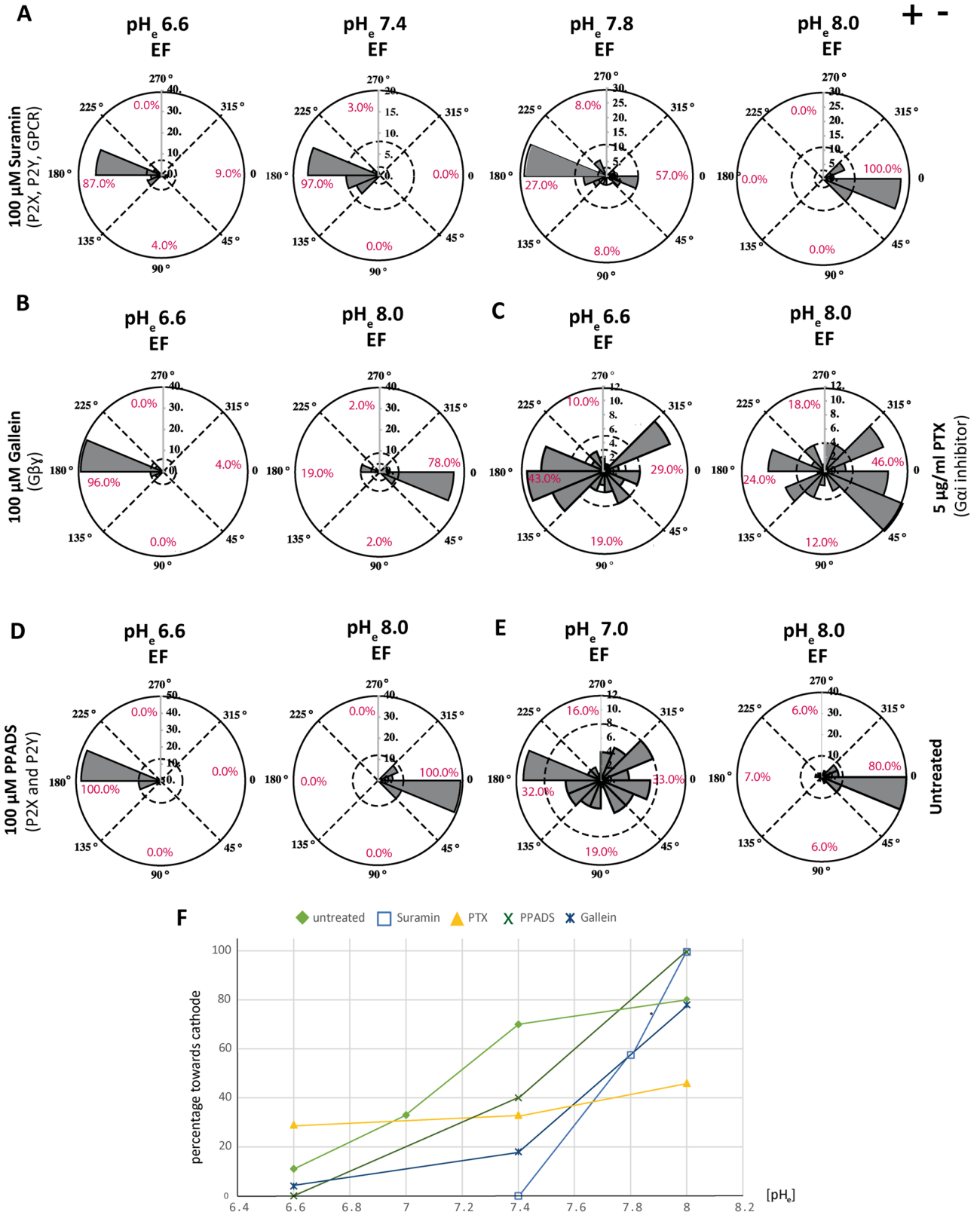

FIGURE 6: Interplay of membrane signaling with pH_e in the EF response. (A–D) Rose plots representing the direction of symmetry breaking with indicated inhibitors and doses at the indicated pH_e values. (A) Suramin treatment leads to anodal polarization at pH_e 6.6, 7.4, and 7.8. At pH_e 8.0, cathodal polarization is restored. (B) Cathodal polarization is also restored for Gallein treatment at pH_e 8.0. (C) Gαi inhibition with PTX shows anodal bias at low pH (pH_e 6.6) and cathodal bias at high pH (pH_e 8.0). (D) Cathodal polarization in PPADS-treated cells at high pH_e. (E) Untreated cells show randomization at pH_e 7.0 and strong cathodal polarization at pH_e 8.0. (F) Graph showing percentage of cathodal polarization at different pH_e values. Different symbols represent different treatments.

contractility to break symmetry despite the fact that they have a similar morphology (Yam *et al.*, 2007). An interesting finding was that EF stimulation increased the percentage of Rac1- and Arp2/3-inhibited cells capable of symmetry breaking. This suggested that the EF evoked compensatory polarization pathways. An alternative explanation is that the pharmacological treatments did not cause a complete loss of function and that the upstream cathodal directionality sensors were able to concentrate and thus increase their localized activity. A similar process may be at work when random polarization is overridden by EF-dependent polarization.

Our findings also allow the conclusion that directionality instructions were generated upstream of the intracellular actin-associated factors, because their inhibition did not interfere with the direction of symmetry breaking. On the contrary, all of the treatments that affected directionality targeted plasma membrane molecules. This fits well with the notion that the EF effects should be confined to the outer surface of the plasma membrane due to the high resistance of the plasma membrane (Poo, 1981). Randomization of directionality occurred when EGFR was inhibited. Reversal of directionality from cathode to anode was achieved by low extracellular pH, GPCR and purinergic signaling, and, partially, PI3K inhibition. Of great interest, there seemed to be a pH_e-dependent spectrum of phenotypes. Some treatments (PTX and PPADS) showed anodal polarization at pH_e 6.5, randomization at pH_e 7.4, and cathodal polarization at pH_e 8. For others (suramin, gallein), this spectrum was shifted toward even higher pH values. Because anodal polarization was still seen at neutral pH_e, this suggests that the anodal pathway was more potent than in untreated cells. In other words, the outcome of the tug-of-war was in favor of the anodal pathway because important cathodal factors were eliminated.

What are these cathodal factors? In addition to antagonism of P2 receptors, suramin inhibits the activation of heterotrimeric G proteins in a variety of GPCRs with varying potency. Because gallein is a general inhibitor of Gβγ subunits, it might be that broad inhibition of GPCR signaling is causing the observed reversal phenotype. However, the overlap between the proposed inhibitor effects argues for a particularly important role of the P2Y receptor class, which is the only set of GPCRs within the purinergic system. This is in accordance with a recent report on the role of purinergic signaling in electrotaxis of primary keratinocytes (Riding and Pullar, 2015). Here suramin caused randomization and not reversal of migration, suggesting once again that our polarization assay is more suited than electrotaxis to dissect mechanisms of cathodal versus anodal pathways.

Although the pharmacological treatments discussed here might have targeted a dedicated cathodal directionality system, the components of the anodal pathway are entirely unclear. It could be argued, however, that the reversal phenotype depends on a drift of molecules on the cell surface controlled by the overall surface charge density and the charge on specific molecules (McLaughlin and Poo, 1981; Allen *et al.*, 2013). The principle has been demonstrated for EGF (Giugni *et al.*, 1987; Fang *et al.*, 1999), low density lipoprotein (Tank *et al.*, 1985), acetylcholine receptor (Orida and Poo, 1978), and concanavalin A–binding receptors (McLaughlin and Poo, 1981). In this manner, anodal polarization would not be achieved by an anodal pathway but by the anodal localization of cathodal pathway components. However, our data give evidence against this scenario. First, the reversal of polarization in low pH_e appeared morphologically different than with normal pH_e. Second, we showed that the anodal pathway becomes dominant over the cathodal pathway when cathodal players are inhibited. To obtain a more complete picture of the regulation of directionality, treatments that change surface charges could be combined with the direct visualization of a set of chosen surface receptors, such as P2Y receptors. Similarly, the contribution of a specific molecule to directionality could be tested by artificially changing the quantity of charges on the extracellular domain. We believe that our polarization assay represents a very useful resource for efforts to tackle the question of EF sensing.

We further expect our findings to have a number of direct implications for epidermal wound healing. All signaling systems targeted here have previously been shown to play a role in keratinocyte electrotaxis and/or wound healing in vivo (Pullar and Isseroff, 2005; Gault *et al.*, 2014). Given that EGFR can be transactivated by GPCRs during wound healing (Yin *et al.*, 2007), there may also be significant cross-talk between the individual signaling receptors. Furthermore, it is important to note that nonhealing chronic wounds display extracellular pH gradients with lower pH values at the wound periphery (Schreml *et al.*, 2014). This could imply that signaling pathways driving the cells toward the wound center may be impaired at low pH, causing randomization and even reversal of polarization and migration. Additional studies are required to investigate whether the modification of the pH environment, such as with dynamic hydrogels, could be a therapeutic alternative for chronic wounds (Burdick and Murphy, 2012; Schreml *et al.*, 2014).

MATERIALS AND METHODS

Cell culture and pharmacological treatments

Keratinocytes (courtesy of Leena Bruckner-Tuderman, Department of Dermatology, University Hospital Freiburg) isolated from human foreskin were transformed with the human papillomavirus oncogenes E6 and E7 for immortalization (Kaur and McDougall, 1988). Cells were kept in Keratinocyte Serum-Free Medium (KSFM; Invitrogen, Carlsbad, CA) supplemented with 0.3 ng/ml recombinant EGF and 30 ng/ml bovine pituitary extract and 100 U/ml penicillin/streptomycin (culture medium). The experiment medium contained an additional 20 mM 4-(2-hydroxyethyl)-1-piperazineethanesulfonic acid (Sigma-Aldrich, St. Louis, MO). For pH experiments, the medium was adjusted to a pH of 7.45 by 2.5 N NaOH or to 6.6 by 10% HCl. The inhibitors CK-666 (Sigma-Aldrich), NSC-23766 (Tocris, Bristol, UK), ZCL-278 (Tocris), PIK-90 (Selleck Chemicals, Houston, TX), AG-1478 (Cayman Chemicals, Ann Arbor, MI), Y-27632 (Merck-Millipore, Billerica, MA), (–)-blebbistatin (Sigma-Aldrich), suramin (Tocris), pertussis toxin (Enzo Scientific, Farmingdale, NY), gallein (Tocris), telenzepine (Tocris), PPADS (Tocris), and CK-689 (Merck-Millipore) were used at the indicated concentrations.

Polarization assay and phase-contrast microscopy

Ibidi µ-channel slides were coated with collagen type I from rat tail (Life Technologies, Carlsbad, CA) diluted in 0.02 M acetic acid (Carl Roth, Karlsruhe, Germany) at a ratio of 1:40 (vol/vol) for 1 h at room temperature. Slides were washed with phosphate-buffered saline (PBS; Pan, Aidenbach, Germany) and dried for 15 min before seeding. Keratinocytes were seeded at 15,000 cells per µ-channel slide. Cells were incubated for a minimum of 24 h and a maximum of 48 h before the experiment until they obtained their characteristic half-moon shape. For the polarization assay, the culture medium was replaced with the experiment medium supplemented with 8% DMSO (Sigma-Aldrich). Cells were allowed to round up for 30 min. The DMSO-containing medium was washed off with 2–3 ml of experiment medium containing either the vehicle control or inhibitors. For EF-controlled polarization, cells in the µ-channel slides were exposed to the EF after the DMSO washout. Thus slides were connected to the voltage supply via silicon tubes filled with a mixture of 2% agarose (Carl Roth) in KSFM. Ag/AgCl disk electrodes

(Science Products, Hofheim, Germany) were placed in the electrolyte solution of 3 M KCl and connected to a programmable voltage supply (Agilent, Santa Clara, CA). Two platinum wires (World Precision Instruments, Saratosa, FL) were placed in each well of the channel slide to record the potential drop across the channel and were connected to a voltage feedback system to keep the potential drop across the channel slide at 5 V (100 mV/mm × 5 cm). Cell spreading, symmetry breaking, and subsequent migration were recorded for 1.5 h with 1-min time interval at 10 different positions. Imaging was performed with a Zeiss Cell Observer microscope controlled by AxioVision and equipped with a cooled charge-coupled device AxioCam Rev3 camera. An EC Plan Neofluar 20×/0.5 phase contrast objective (Zeiss, Oberkochen, Germany) was used. All experiments were carried out at 37°C.

Directionality analysis

Three types of information were collected from each cell recorded in the 1.5 h after DMSO removal: one was the categorization of the type of polarization (see legends in the corresponding figures), represented as percentages in bar charts. Cells were categorized manually by following cell behavior in videos. All quantified cells fell under one of the following four categories. Cells that did not change axis of polarity after polarization were termed "stable polarity axis." The "unstable polarity axis" category corresponded to cells that changed morphology by retracting the lamellipodium formed after symmetry breaking and creating another one elsewhere at the cell periphery. Cells in the ">1 lamellipodium" category had either a stable or an unstable polarity axis, but their major characteristic was that they had more than one lamellipodial structure. Cells that failed to polarize were termed "unpolarized." Cells in the first three categories successfully polarized. The second type of information was the time it takes to for the cell to polarize after the DMSO wash. The graphs for the polarization time were constructed in Mathematica, such that each black dot represented one single cell analyzed. Third, for a directionality experiment, the angle at which cells position the midpoint of their lamellipodium was extracted. The 0° position was designated to be the cathodal side of the horizontal line drawn parallel to the direction of the EF. A second line was drawn along the lagging edge of the polarized cell. The midpoint of the lamellipodium was connected to the intersection of the 0° line and the lagging-edge line with a third line. The angle between the 0° line and the third, mid-lamellipodium line was measured with a protractor and recorded. The recorded angles were displayed on rose plots constructed in Mathematica around the SectorChart command. Polar axes were divided into 16 polar grids, and values for the directionality angle for each cell that falls into these grids were binned. The percentage of cells that break symmetry toward four different directions (up, down, cathode, and anode) was calculated by grouping the 16 grids into groups of four.

All experiments were performed at least in duplicate, with similar results. For directionality experiments with inhibitors, a control EF experiment was always run on the same day. For quantifications, representative experiments were used, and the data shown originate from either a single experiment or a combination of experiments from different days. For each video recorded, cells that did not have any touching neighbors were quantified. The number of cells analyzed for each condition is stated in polarization-type charts and rose plots. All statistics were computed in Mathematica. Statistics on polarization types were performed on the polarization type that mattered most between the conditions. From the percentage value of the polarization type and the number of analyzed cells (N), the Bernoulli distribution was computed. Random variates from the computed distributions were analyzed with a Student's t test for the mean of distributions. For the polarization-time data, the test type was selected automatically according to the distribution (Student's t test or Mann–Whitney test). The testing was done to compare the mean of distributions. The statistics on polarization angles were done as for the polarization types.

Automated cell tracking

For some experiments, we followed the tracks of cells after they broke symmetry. The cell-tracking program was home-written in Mathematica around the Dynamic command. Every 10th image was loaded and made into a series that was under the control of a slider. The program recorded the (x, y) coordinates of each click (center of the nucleus) on each image from which a cell track was constructed. Tracking started 10 min after the DMSO wash and ended at 1.5 h after the wash. All tracked cells were shown together on a set of xy-axes after the starting point of each cell track was brought to the (0, 0) coordinate. The directionality index, $\cos\theta$, of a migrating cell was calculated using the x and y displacements of cells from start to finish. The displacement value is the shortest distance from the start to the end coordinates in the time window tracked, and the track length is the summation of the displacement values calculated between every 10th image in the tracking series. The straightness value was obtained by dividing the track length with the displacement for each cell.

Intracellular and extracellular pH measurements

For intracellular pH measurements, cells were transfected with a superecliptic pHluorin-mCherry construct (32001; Addgene; Koivusalo *et al.*, 2010), using FuGENE HG (Roche, Basel, Switzerland). Superecliptic pHluorin and mCherry excitation was recorded simultaneously using the dual-camera mode of the Zeiss observer microscope (dual-filter set 79 HE; Zeiss) with an Alpha-Plan-Apochromat 100×/1.46 objective. Calibration was performed at the end of each experiment with nigericin (Sigma-Aldrich) containing K^+-rich calibration solution (143 mM KCl, 1 mM $MgCl_2$, 1 mM $CaCl_2$, 5 mM glucose, 10 μg/ml nigericin) at three pH values between 6.8 and 7.8. Postprocessing of raw fluorescence data was done with a self-written Mathematica program. Background value was subtracted from raw images, followed by filtering with a Gaussian filter of value 3. The ratiometric image was obtained by dividing the pHluorin image by the mCherry image. Image masks were created by thresholding for every image. For calibration images, pixel values were averaged from masked images, and average pixel value versus the corresponding pH value was graphed. A linear equation was fitted to the curve. The pixel-to-pixel intensities of the masked ratiometric images were converted to pH values using the obtained equation. For experiments in which pH values were averaged from different cells, cells from a single experiment were used.

For extracellular pH measurements, μ-channel slides were filled with experiment medium supplemented with 10 μM BCECF acid (Life Technologies). Four positions were selected on the slide for testing whether an extracellular pH gradient formed during EF application. Images were taken every 30 s using a Zeiss Cell Observer microscope equipped with a custom BCECF filter (excitation, bandpass 460/80 nm; beam splitter, 506 nm; emission, bandpass 578/105 nm) and EC Plan Neofluar 20×/0.5 objective (Zeiss). Illumination was provided by a monochromator (Till Photonics) at λ_1 = 490 nm and λ_2 = 440 nm. Analysis was done in Mathematica. A calibration curve was generated by using BCECF acid–supplemented experiment medium at three pH values between 6.8 and

7.8. The ratio images were obtained by dividing raw fluorescence images (λ_2/λ_1) after subtraction of the background. Absolute pH values were calculated using the equation obtained from the calibration curve. Each condition was repeated three times.

Actin cytoskeleton visualization

For live imaging of F-actin, cells were transfected with the Lifeact-mCherry construct (courtesy of D. Müller, ETH, Basel, Switzerland) using FuGENE HG (Roche). A Zeiss Cell Observer microscope was used to image cells equipped with a 43 HE filter (Zeiss) and Alpha-Plan-Fluar 100×/1.45 oil immersion objective (Zeiss). Images were recorded at 2-min time intervals and subjected to postprocessing using the online version of Huygens deconvolution software to eliminate the out-of-focus fluorescence.

In addition, untreated and CK-666– and CK-689–treated cells were fixed with 4% paraformaldehyde for 15 min in the dark, followed by PBS wash. Cells were then stained with Alexa Fluor 488–phalloidin (Life Technologies) for 20 min and washed with PBS. Imaging was performed with a Zeiss Cell Observer microscope equipped with a 43 HE filter (Zeiss) Alpha-Plan-Fluar 100×/1.45 oil immersion objective (Zeiss). Images were postprocessed with the Huygens deconvolution software to eliminate the out-of-focus fluorescence.

Protein extraction and Western blotting

Cells were seeded at a nonconfluent density on 10-mm plates coated with collagen I. Cells were washed with ice-cold PBS, and cellular protein in treated and untreated samples was extracted using a 150 µl of RIPA buffer on the dish 10, 30, and 60 min after DMSO removal. Cellular extracts were kept on ice for 5 min, and 5× Laemmli buffer was added. The samples that were blotted for ppMRLC2 contained an additional 1 mM ATP. Extracts were boiled for 15 min before loading on 4–12% gradient gels (GenScript, Piscataway, NJ). Wet transfer was performed onto polyvinylidene fluoride membranes. The primary antibodies ppMRLC2, pEGFR (Tyr-992), EGFR, α-tubulin, and β-actin (all Cell Signaling) were used at 1/1000 concentration in 5% milk in PBS/Tween-20 (0.02%). The secondary antibody anti-rabbit (Cell Signaling) was used at 1/2000 (Cell Signaling) and anti-mouse (Bethyl, Montomery, TX) at 1/5000 in PBS.

Protrusion/retraction velocity maps

Cell outlines were calculated using graph cut segmentation (Boykov and Kolmogorov, 2004). To obtain a consistent temporal segmentation, segmentation information was propagated between frames. Graph cut unary costs were set to zero, except for pixels with hard foreground/background constraints, for which unary costs were set to a sufficiently large constant *K*. For computing boundary costs, we chose asymmetric penalties. This promotes segmentations along dark–bright intensity transitions that are characteristic at cell boundaries in phase contrast microscopy (Bensch and Ronneberger, 2015). For initialization, dark spots inside the cells were used as foreground mask, computed by thresholding. Starting from the initial segmentation, segmentation information was propagated to the next frame. The eroded segmentation mask served as hard foreground constraint, and the complement of the dilated segmentation mask served as hard background constraint for the segmentation of the next frame. In a postprocessing step, small segments were discarded, and cell outlines were smoothed. Automated cell outline determination yielded precise results; however, outlines were manually inspected to ensure high-quality results and manually corrected where necessary.

Symmetry-breaking events were detected to assist in browsing the large amount of data and extract relevant time intervals. When cells break symmetry, their shape changes from a roundish to an elliptic shape. We identify symmetry-breaking events by detecting these shape transitions. For each cell segment, the eccentricity was computed as a function over time. The eccentricity is the ratio of the distance between the foci of an ellipse (with the same second moments as the segment) and its major axis length. It is 0 for a circle and 1 for an ellipse that is degenerated to a line segment. To this end, frame intervals where the eccentricity traverses the range [0.6, 0.7] were detected as symmetry-breaking events. A reference orientation was computed at the frame where eccentricity was closest to 0.7.

Protrusion/retraction velocity maps describe cell contour movements in a polar coordinate system and distinguish outward- (protrusion) and inward-pointing movements (retraction). Contours were extracted as the boundary pixel positions of the cell segments. For cells breaking symmetry, the orientation was normalized to the reference orientation computed before. For calculating cell contour movements, we established temporal point correspondences by uniform angular sampling ($N = 80$ angular samples) of the contours centered to their mean position. Contour positions were smoothed temporally to compensate for inconsistent fluctuations. Contour velocity vectors were computed from the displacement vectors between corresponding contour points. Cell edge protrusion/retraction was measured by the scalar projection of the velocity vectors onto the local normal direction of the cell contour (normal direction defined as pointing outward). The measure is positive for protrusion and negative for retraction.

The methods were implemented in MATLAB (MathWorks). Eccentricity and orientation were computed by MATLAB function regionprops. Graph cut segmentation was computed using the MATLAB interface provided by Boykov and Kolmogorov (2004).

ACKNOWLEDGMENTS

We are grateful to Roland Nitschke and the Life Imaging Centre (LIC) team for help with microscopy. We thank Nicolas Minc, William Gault, and Michael Köttgen for critically reading the manuscript. We are grateful to Daniel Müller for the LifeAct-mCherry construct. This work has been supported by Emmy-Noether Grant SI1303/2-1, the German Federal Ministry for Education and Research FORSYS Program 0313921 (FRISYS), the Excellence Initiative of the German Federal and State Governments (BIOSS EXC 294), and the Excellence Initiative of the German Research Foundation (GSC-4, Spemann Graduate School).

REFERENCES

Allen GM, Mogilner A, Theriot JA (2013). Electrophoresis of cellular membrane components creates the directional cue guiding keratocyte galvanotaxis. Curr Biol 23, 560–568.

Beindl W, Mitterauer T, Hohenegger M, Ijzerman AP, Nanoff C, Freissmuth M (1996). Inhibition of receptor/G protein coupling by suramin analogues. Mol Pharmacol 50, 415–423.

Bensch R, Ronneberger O (2015). Cell segmentation and tracking in phase contrast images using graph cut with asymmetric boundary costs. IEEE Int Symp Biomed Imaging, 2015, 1220–1223.

Borgens RB, Vanable JW Jr, Jaffe LF (1977). Bioelectricity and regeneration: large currents leave the stumps of regenerating newt limbs. Proc Natl Acad Sci USA 74, 4528–4532.

Bourne HR, Weiner O (2002). A chemical compass. Nature 419, 21.

Boykov Y, Kolmogorov V (2004). An experimental comparison of min-cut/max-flow algorithms for energy minimization in vision. IEEE Trans Pattern Anal Machine Intell 26, 1124–1137.

Burdick JA, Murphy WL (2012). Moving from static to dynamic complexity in hydrogel design. Nat Commun 3, 1269.

Cao L, Wei D, Reid B, Zhao S, Pu J, Pan T, Yamoah E, Zhao M (2013). Endogenous electric currents might guide rostral migration of neuroblasts. EMBO Rep 14, 184–190.
Chang F, Minc N (2014). Electrochemical control of cell and tissue polarity. Annu Rev Cell Dev Biol 30, 317–336.
Chiang M, Robinson KR, Vanable JW, Jr (1992). Electrical fields in the vicinity of epithelial wounds in the isolated bovine eye. Exp Eye Res 54, 999–1003.
Cohen DJ, Nelson WJ, Maharbiz MM (2014). Galvanotactic control of collective cell migration in epithelial monolayers. Nat Mater 13, 409–417.
Fang KS, Ionides E, Oster G, Nuccitelli R, Isseroff RR (1999). Epidermal growth factor receptor relocalization and kinase activity are necessary for directional migration of keratinocytes in DC electric fields. J Cell Sci 112, 1967–1978.
Ferrier J, Ross SM, Kanehisa J, Aubin JE (1986). Osteoclasts and osteoblasts migrate in opposite directions in response to a constant electrical field. J Cell Physiol 129, 283–288.
Friesland A, Zhao Y, Chen YH, Wang L, Zhou H, Lu Q (2013). Small molecule targeting Cdc42-intersectin interaction disrupts Golgi organization and suppresses cell motility. Proc Natl Acad Sci USA 110, 1261–1266.
Gao Y, Dickerson JB, Guo F, Zheng J, Zheng Y (2004). Rational design and characterization of a Rac GTPase-specific small molecule inhibitor. Proc Natl Acad Sci USA 101, 7618–7623.
Gault WJ, Enyedi B, Niethammer P (2014). Osmotic surveillance mediates rapid wound closure through nucleotide release. J Cell Biol 207, 767–782.
Giugni TD, Braslau DL, Haigler HT (1987). Electric field-induced redistribution and postfield relaxation of epidermal growth factor receptors on A431 cells. J Cell Biol 104, 1291–1297.
Heasman SJ, Ridley AJ (2008). Mammalian Rho GTPases: new insights into their functions from in vivo studies. Nat Rev Mol Cell Biol 9, 690–701.
Ho E, Dagnino L (2012). Epidermal growth factor induction of front-rear polarity and migration in keratinocytes is mediated by integrin-linked kinase and ELMO2. Mol Biol Cell 23, 492–502.
Hotary KB, Robinson KR (1994). Endogenous electrical currents and voltage gradients in Xenopus embryos and the consequences of their disruption. Dev Biol 166, 789–800.
Jaffe AB, Hall A (2005). Rho GTPases: biochemistry and biology. Annu Rev Cell Dev Biol 21, 247–269.
Jaffe LF, Stern CD (1979). Strong electrical currents leave the primitive streak of chick embryos. Science 206, 569–571.
Jahn T (1961). The mechanism of ciliary movement. I. Ciliary reversal and activation by electric current; the ludloff phenomenon in terms of core and volume conductors. J Protozool 8, 369–380.
Kaur P, McDougall JK (1988). Characterization of primary human keratinocytes transformed by human papillomavirus type 18. J Virol 62, 1917–1924.
Keren K, Pincus Z, Allen GM, Barnhart EL, Marriott G, Mogilner A, Theriot JA (2008). Mechanism of shape determination in motile cells. Nature 453, 475–480.
Knight ZA, Gonzalez B, Feldman ME, Zunder ER, Goldenberg DD, Williams O, Loewith R, Stokoe D, Balla A, Toth B, *et al*. (2006). A pharmacological map of the PI3-K family defines a role for p110alpha in insulin signaling. Cell 125, 733–747.
Koivusalo M, Welch C, Hayashi H, Scott CC, Kim M, Alexander T, Touret N, Hahn KM, Grinstein S (2010). Amiloride inhibits macropinocytosis by lowering submembranous pH and preventing Rac1 and Cdc42 signaling. J Cell Biol 188, 547–563.
Lauffenburger DA, Horwitz AF (1996). Cell migration: a physically integrated molecular process. Cell 84, 359–369.
Levin M (2009). Bioelectric mechanisms in regeneration: unique aspects and future perspectives. Semin Cell Dev Biol 20, 543–556.
Li R, Gundersen GG (2008). Beyond polymer polarity: how the cytoskeleton builds a polarized cell. Nat Rev Mol Cell Biol 9, 860–873.
Martin C, Pedersen SF, Schwab A, Stock C (2011). Intracellular pH gradients in migrating cells. Am J Physiol Cell Physiol 300, C490–C495.
McLaughlin S, Poo MM (1981). The role of electro-osmosis in the electric-field-induced movement of charged macromolecules on the surfaces of cells. Biophys J 34, 85–93.
Minc N, Chang F (2010). Electrical control of cell polarization in the fission yeast Schizosaccharomyces pombe. Curr Biol 20, 710–716.
Orida N, Poo MM (1978). Electrophoretic movement and localisation of acetylcholine receptors in the embryonic muscle cell membrane. Nature 275, 31–35.
Patel N, Poo MM (1982). Orientation of neurite growth by extracellular electric fields. J Neurosci 2, 483–496.
Poo M (1981). In situ electrophoresis of membrane components. Annu Rev Biophys Bioeng 10, 245–276.
Pu J, McCaig CD, Cao L, Zhao Z, Segall JE, Zhao M (2007). EGF receptor signalling is essential for electric-field-directed migration of breast cancer cells. J Cell Sci 120, 3395–3403.
Pullar CE, Isseroff RR (2005). Cyclic AMP mediates keratinocyte directional migration in an electric field. J Cell Sci 118, 2023–2034.
Rapp B, de Boisfleury-Chevance A, Gruler H (1988). Galvanotaxis of human granulocytes. Dose-response curve. Eur Biophys J 16, 313–319.
Reid B, Nuccitelli R, Zhao M (2007). Non-invasive measurement of bioelectric currents with a vibrating probe. Nat Protoc 2, 661–669.
Riding A, Pullar CE (2015). ATP release and P2Y receptor signalling are essential for keratinocyte galvanotaxis. J Cell Physiol 231, 181–191.
Sanger JW, Gwinn J, Sanger JM (1980). Dissolution of cytoplasmic actin bundles and the induction of nuclear actin bundles by dimethyl sulfoxide. J Exp Zool 213, 227–230.
Sato MJ, Kuwayama H, van Egmond WN, Takayama AL, Takagi H, van Haastert PJ, Yanagida T, Ueda M (2009). Switching direction in electric-signal-induced cell migration by cyclic guanosine monophosphate and phosphatidylinositol signaling. Proc Natl Acad Sci USA 106, 6667–6672.
Schreml S, Meier RJ, Kirschbaum M, Kong SC, Gehmert S, Felthaus O, Kuchler S, Sharpe JR, Woltje K, Weiss KT, *et al*. (2014). Luminescent dual sensors reveal extracellular pH-gradients and hypoxia on chronic wounds that disrupt epidermal repair. Theranostics 4, 721–735.
Soong HK, Parkinson WC, Sulik GL, Bafna S (1990). Effects of electric fields on cytoskeleton of corneal stromal fibroblasts. Curr Eye Res 9, 893–901.
Srinivasan S, Wang F, Glavas S, Ott A, Hofmann F, Aktories K, Kalman D, Bourne HR (2003). Rac and Cdc42 play distinct roles in regulating PI(3,4,5)P3 and polarity during neutrophil chemotaxis. J Cell Biol 160, 375–385.
Sun Y, Do H, Gao J, Zhao R, Zhao M, Mogilner A (2013). Keratocyte fragments and cells utilize competing pathways to move in opposite directions in an electric field. Curr Biol 23, 569–574.
Tank DW, Fredericks WJ, Barak LS, Webb WW (1985). Electric field-induced redistribution and postfield relaxation of low density lipoprotein receptors on cultured human fibroblasts. J Cell Biol 101, 148–157.
Wang E, Zhao M, Forrester JV, McCaig CD (2003). Bi-directional migration of lens epithelial cells in a physiological electrical field. Exp Eye Res 76, 29–37.
Yam PT, Wilson CA, Ji L, Hebert B, Barnhart EL, Dye NA, Wiseman PW, Danuser G, Theriot JA (2007). Actin-myosin network reorganization breaks symmetry at the cell rear to spontaneously initiate polarized cell motility. J Cell Biol 178, 1207–1221.
Yang HY, Charles RP, Hummler E, Baines DL, Isseroff RR (2013). The epithelial sodium channel mediates the directionality of galvanotaxis in human keratinocytes. J Cell Sci 126, 1942–1951.
Yin J, Xu K, Zhang J, Kumar A, Yu FS (2007). Wound-induced ATP release and EGF receptor activation in epithelial cells. J Cell Sci 120, 815–825.
Zhao M (2009). Electrical fields in wound healing—an overriding signal that directs cell migration. Semin Cell Dev Biol 20, 674–682.
Zhao M, Bai H, Wang E, Forrester JV, McCaig CD (2004). Electrical stimulation directly induces pre-angiogenic responses in vascular endothelial cells by signaling through VEGF receptors. J Cell Sci 117, 397–405.
Zhao M, Jin T, McCaig CD, Forrester JV, Devreotes PN (2002a). Genetic analysis of the role of G protein-coupled receptor signaling in electrotaxis. J Cell Biol 157, 921–927.
Zhao M, Pu J, Forrester JV, McCaig CD (2002b). Membrane lipids, EGF receptors, and intracellular signals colocalize and are polarized in epithelial cells moving directionally in a physiological electric field. FASEB J 16, 857–859.
Zhao M, Song B, Pu J, Wada T, Reid B, Tai G, Wang F, Guo A, Walczysko P, Gu Y, *et al*. (2006). Electrical signals control wound healing through phosphatidylinositol-3-OH kinase-gamma and PTEN. Nature 442, 457–460.